Chalmers Publication Library

Copyright Notice

(Article begins on next page)

Mode-specific directional emission from hybridized particle-on-a-film plasmons

Vladimir D. Miljković,[1,*] Timur Shegai,[1] Mikael Käll,[1] and Peter Johansson[1,2]

[1]Department of Applied Physics, Chalmers University of Technology, 412 96 Göteborg, Sweden
[2]School of Science and Technology, Örebro University, 701 82 Örebro, Sweden
*vladimir.miljkovic@chalmers.se

Abstract: We investigate the electromagnetic interaction between a gold nanoparticle and a thin gold film on a glass substrate. The coupling between the particle plasmons and the surface plasmon polaritons of the film leads to the formation of two localized hybrid modes, one low-energy "film-like" plasmon and one high-energy plasmon dominated by the nanoparticle. We find that the two modes have completely different directional scattering patterns on the glass side of the film. The high-energy mode displays a characteristic dipole emission pattern while the low-energy mode sends out a substantial part of its radiation in directions parallel to the particle dipole moment. The relative strength of the two radiation patterns vary strongly with the distance between the particle and the film, as determined by the degree of particle-film hybridization.

References and links

1. M. Moskovits, "Surface-enhanced spectroscopy," Rev. Mod. Phys. **57**(3), 783–826 (1985).
2. S. Lal, S. Link, and N. J. Halas, "Nano-optics from sensing to waveguiding," Nat. Photonics **1**(11), 641–648 (2007).
3. H. A. Atwater and A. Polman, "Plasmonics for improved photovoltaic devices," Nat. Mater. **9**(3), 205–213 (2010).
4. E. Kretschmann and H. Raether, "Radiative decay of radiative surface plasmons excited by light," Z. Naturforsch., A **23**, 2135–2136 (1968).
5. P. K. Aravind and H. Metiu, "The effects of the interaction between resonances in the electromagnetic response of a sphere-plane structure—applications to surface enhanced spectroscopy," Surf. Sci. **124**(2-3), 506–528 (1983).
6. R. Ruppin, "Surface modes and optical absorption of a small sphere above a substrate," Surf. Sci. **127**(1), 108–118 (1983).
7. W. R. Holland and D. G. Hall, "Frequency-shifts of an electric-dipole resonance near a conducting surface," Phys. Rev. Lett. **52**(12), 1041–1044 (1984).
8. R. Berndt, J. K. Gimzewski, and P. Johansson, "Inelastic tunneling excitation of tip-induced plasmon modes on noble-metal surfaces," Phys. Rev. Lett. **67**(27), 3796–3799 (1991).
9. B. Lamprecht, G. Schider, R. T. Lechner, H. Ditlbacher, J. R. Krenn, A. Leitner, and F. R. Aussenegg, "Metal nanoparticle gratings: influence of dipolar particle interaction on the plasmon resonance," Phys. Rev. Lett. **84**(20), 4721–4724 (2000).
10. P. Johansson, "Light scattering from disordered overlayers of metallic nanoparticles," Phys. Rev. B **64**(16), 165405 (2001).
11. T. Okamoto and I. Yamaguchi, "Optical absorption study of the surface plasmon resonance in gold nanoparticles immobilized onto a gold substrate by self-assembly technique," J. Phys. Chem. B **107**(38), 10321–10324 (2003).
12. P. Nordlander and E. Prodan, "Plasmon hybridization in nanoparticles near metallic surfaces," Nano Lett. **4**(11), 2209–2213 (2004).
13. F. Le, N. Z. Lwin, J. M. Steele, M. Käll, N. J. Halas, and P. Nordlander, "Plasmons in the metallic nanoparticle-film system as a tunable impurity problem," Nano Lett. **5**(10), 2009–2013 (2005).
14. G. Lévêque and O. J. F. Martin, "Optical interactions in a plasmonic particle coupled to a metallic film," Opt. Express **14**(21), 9971–9981 (2006).
15. N. Papanikolaou, "Optical properties of metallic nanoparticle arrays on a thin metallic film," Phys. Rev. B **75**(23), 235426 (2007).
16. J. Cesario, M. U. Gonzalez, S. Cheylan, W. L. Barnes, S. Enoch, and R. Quidant, "Coupling localized and extended plasmons to improve the light extraction through metal films," Opt. Express **15**(17), 10533–10539 (2007).

17. A. Rueda, M. Stemmler, R. Bauer, K. Mullen, Y. Fogel, and M. Kreiter, "Optical resonances of gold nanoparticles on a gold surface: quantitative correlation of geometry and resonance wavelength," N. J. Phys. **10**(11), 113001 (2008).
18. J. J. Mock, R. T. Hill, A. Degiron, S. Zauscher, A. Chilkoti, and D. R. Smith, "Distance-dependent plasmon resonant coupling between a gold nanoparticle and gold film," Nano Lett. **8**(8), 2245–2252 (2008).
19. M. Hu, A. Ghoshal, M. Marquez, and P. G. Kik, "Single particle spectroscopy study of metal-film-induced tuning of silver nanoparticle plasmon resonances," J. Phys. Chem. C **114**(16), 7509–7514 (2010).
20. N. Liu, M. Mesch, T. Weiss, M. Hentschel, and H. Giessen, "Infrared perfect absorber and its application as plasmonic sensor," Nano Lett. **10**(7), 2342–2348 (2010).
21. J. Jung, T. Sondergaard, and S. I. Bozhevolnyi, "Gap plasmon-polariton nanoresonators: scattering enhancement and launching of surface plasmon polaritons," Phys. Rev. B **79**(3), 035401 (2009).
22. B. Hecht, H. Bielefeldt, L. Novotny, Y. Inouye, and D. W. Pohl, "Local excitation, scattering, and interference of surface plasmons," Phys. Rev. Lett. **77**(9), 1889–1892 (1996).
23. T. Kume, S. Hayashi, and K. Yamamoto, "Light emission from surface plasmon polaritons mediated by metallic fine particles," Phys. Rev. B **55**(7), 4774–4782 (1997).
24. A. Bouhelier and G. P. Wiederrecht, "Excitation of broadband surface plasmon polaritons: plasmonic continuum spectroscopy," Phys. Rev. B **71**(19), 195406 (2005).
25. C. Nylander, B. Liedberg, and T. Lind, "Gas-detection by means of surface-plasmon resonance," Sens. Actuators **3**, 79–88 (1982).
26. L. A. Lyon, D. J. Pena, and M. J. Natan, "Surface plasmon resonance of Au colloid-modified Au films: particle size dependence," J. Phys. Chem. B **103**(28), 5826–5831 (1999).
27. L. He, M. D. Musick, S. R. Nicewarner, F. G. Salinas, S. J. Benkovic, M. J. Natan, and C. D. Keating, "Colloidal Au-enhanced surface plasmon resonance for ultrasensitive detection of DNA hybridization," J. Am. Chem. Soc. **122**(38), 9071–9077 (2000).
28. M. Svedendahl, S. Chen, A. Dmitriev, and M. Käll, "Refractometric sensing using propagating versus localized surface plasmons: a direct comparison," Nano Lett. **9**(12), 4428–4433 (2009).
29. T. Rindzevicius, Y. Alaverdyan, M. Käll, W. A. Murray, and W. L. Barnes, "Long-range refractive index sensing using plasmonic nanostructures," J. Phys. Chem. C **111**(32), 11806–11810 (2007).
30. A. Dmitriev, C. Hägglund, S. Chen, H. Fredriksson, T. Pakizeh, M. Käll, and D. S. Sutherland, "Enhanced nanoplasmonic optical sensors with reduced substrate effect," Nano Lett. **8**(11), 3893–3898 (2008).
31. B. Brian, B. Sepúlveda, Y. Alaverdyan, L. M. Lechuga, and M. Käll, "Sensitivity enhancement of nanoplasmonic sensors in low refractive index substrates," Opt. Express **17**(3), 2015–2023 (2009).
32. M. Käll, H. X. Xu, and P. Johansson, "Field enhancement and molecular response in surface-enhanced Raman scattering and fluorescence spectroscopy," J. Raman Spectrosc. **36**(6-7), 510–514 (2005).
33. J. D. Driskell, R. J. Lipert, and M. D. Porter, "Labeled gold nanoparticles immobilized at smooth metallic substrates: systematic investigation of surface plasmon resonance and surface-enhanced Raman scattering," J. Phys. Chem. B **110**(35), 17444–17451 (2006).
34. W. H. Park, S. H. Ahn, and Z. H. Kim, "Surface-enhanced Raman scattering from a single nanoparticle-plane junction," ChemPhysChem **9**(17), 2491–2494 (2008).
35. N. H. Kim, S. J. Lee, and M. Moskovits, "Aptamer-mediated surface-enhanced Raman spectroscopy intensity amplification," Nano Lett. **10**(10), 4181–4185 (2010).
36. T. Shegai, B. Brian, V. D. Miljković, and M. Käll, "Angular distribution of surface-enhanced Raman scattering from individual au nanoparticle aggregates," ACS Nano **5**(3), 2036–2041 (2011).
37. P. Johansson, "Electromagnetic Green's function for layered systems: applications to nanohole interactions in thin metal films," Phys. Rev. B **83**(19), 195408 (2011).
38. O. J. F. Martin, A. Dereux, and C. Girard, "Iterative scheme for computing exactly the total field propagating in dielectric structures of arbitrary shape," J. Opt. Soc. Am. A **11**(3), 1073–1080 (1994).
39. L. Novotny and B. Hecht, *Principles of Nano-Optics* (Cambridge University Press, 2006).
40. P. B. Johnson and R. W. Christy, "Optical-constants of noble-metals," Phys. Rev. B **6**(12), 4370–4379 (1972).

1. Introduction

The interaction between light and surface supported nanostructures is a central part of the nanooptics field and of huge importance for a variety of applications [1–3]. A special case of fundamental interest to the plasmonics research area is when an isolated metal nanostructure that breaks translational invariance interacts with an extended metal surface. One then have to consider the coupling of light to two types of interacting plasmons: the surface plasmon polaritons (SPP's), that is electron density oscillations bound to but free to move along the surface [4], and localized surface plasmons (LSP's) that are confined to a volume close to the nanostructure. Early work in this area focused on analyzing interactions between discrete metal structures and surfaces mainly through image dipole theory [5–7] and inspired a wealth of studies over the years [6,8–21]. Still the directional properties of the light scattered or emitted from nanostructures near metal films have received relatively little attention, although a number of such studies do exist [22–24]. In this paper, we theoretically address the

directional properties of the light scattered from a nanoparticle placed near a metal film as a function of photon energy, geometry, and dielectric environment.

Our starting point is an investigation of the interplay between the particle-film hybrid modes and the plasmon dispersion relation of the metal film. The interaction between the localized particle plasmons and the surface plasmon continuum of the film typically yields spectra with two resonances, one low-energy "film-like" mode and a high-energy mode predominantly localized to the particle. We found that these modes have highly characteristic scattering patterns, a finding that is both of fundamental interest and could have practical use. One possible application is in surface plasmon refractive index sensing. SPP modes are extremely sensitive to the dielectric function of the surrounding, which is the basic phenomenon behind bio/chemo SPR sensors [25]. However, several studies have focused on enhancing the sensitivity even further through coupling with metal nanoparticles [26,27]. Similarly, the nanoparticle LSP modes themselves can be highly effective bio/chemo sensors [28] but their sensing characteristics are strongly affected by substrate interactions [29–31]. Another application is surface-enhanced spectroscopy on molecules embedded in narrow gaps between metal surfaces [5,32], which include several recent reports on particle-on-a-film structures [33–35]. Understanding the angular emission properties of such hybridized systems is highly important from a collection efficiency point-of-view, as we have recently demonstrated for SERS active particle aggregates on dielectric interfaces [36]. However, it is also possible that the intricate SPP-LSP coupling could be utilized for developing completely new analysis methods based on angular emission properties rather than spectra.

2. Methods

All calculations involving a spherical nanoparticle are done using Mie theory in the presence of a layered background [10], i.e. we primarily calculate the electromagnetic field at the surface of the nanoparticle, expressed in terms of vector spherical harmonics which are coupled by the interaction mediated by the metal film and glass substrate. The surface response of the substrate in this case is dealt with through the layered Green's function method [37]. The maximal angular momentum of the multipoles accounted for was set to l_{max} = 50 to establish a certain safety margin. In the typical cases considered here l_{max} = 5 yields very accurate results for the scattered fields, while l_{max} = 30 may be required to get very accurate results for the near field between the particle and the film. The calculations involving nanodisks are carried out using the Green function method [37,38], with a mesh of cubic elements with a side of 2 nm. Plasmon dispersion relations are extracted from classical calculations of local density of states [39].

3. Discussion and results

We first investigate the interaction between a spherical gold nanoparticle (radius R = 30 nm) and gold films with thicknesses, t_f = 5, 10, 18 and 50 nm, respectively, resting on a glass substrate. The system is illustrated schematically in the inset of Fig. 1(b). The refractive index of glass is 1.51 and the frequency-dependent dielectric function of gold is taken from Johnson and Christy [40]. A plane wave incident from the air side and polarized in the x-direction impinges on the particle and film at normal incidence.

In order to understand the interaction between the localized particle plasmon and the broad film continuum we need to find the plasmon dispersion relations of the gold film. The dispersion relations have been determined from the maxima in the density of states obtained from the imaginary part of the electromagnetic Green's function of the layered system composed of vacuum, thin metal film and glass substrate. This procedure captures all contributions to the density of states, from both propagating and evanescent waves. The results are shown in Fig. 1(b) for different film thicknesses t_f. We distinguish two modes (different types of waves), the high-energy leaky mode (associated with an asymmetric charge distribution of opposite charges at the two film interfaces) for which the energy shifts are rather small as t_f is varied, and a low-energy bound mode (associated with a symmetric charge distribution in the film). The leaky mode is evanescent in vacuum but propagating in the glass

substrate, whereas the bound mode is evanescent in both of the surrounding media and can therefore only be excited by a localized source such as a defect or a nanoparticle at or near the surface and not by direct excitation by light. For photon energies above 2.4 eV, the plasmon dispersion is not shown. In this frequency range plasmons in gold are rather strongly damped. The overall behavior of the plasmon dispersion relations is dictated by the interaction between the surface plasmons at the air-gold and gold-glass interface, respectively. A thinner film leads to a stronger interaction and thereby a stronger level repulsion between the two hybrid modes. Hence the low-energy mode moves down, and the high-energy mode (slightly) moves up in energy as t_f is decreased.
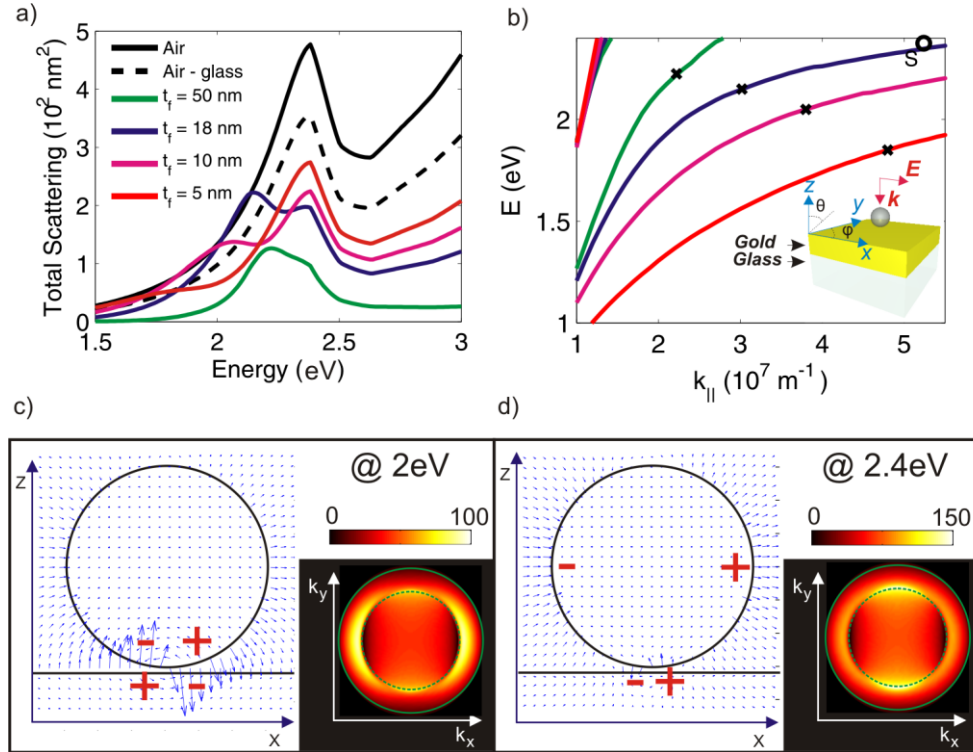

Fig. 1. (a) Calculated scattering spectra for a gold sphere with radius R = 30 nm placed at 1 nm distance from the gold film. In addition, spectra for a particle in air and at an air-glass interface are shown. (b) Dispersion relations for the gold film on a glass substrate calculated for different film thicknesses t_f using the same line colors as in (a) for different thicknesses. (c, d) Real parts of the electric fields $Re\{E_x\}$ and $Re\{E_z\}$ in the xz-plane at 2 eV and 2.4 eV for 10 nm thick films revealing the charge distributions for the low-energy and high-energy modes, respectively. Insets in (c, d) show glass-side radiation patterns in the substrate-side Fourier plane for the two modes.

Figure 1(a) shows total scattering cross sections for scattering to the glass side for a gold sphere illuminated under normal incidence. The black curves show scattering cross sections for a gold particle in free space (black solid line) and at an air-glass interface (black dashed line). The rest of the spectra show total scattering cross sections to the glass side for a gold particle near a gold film on top of a glass substrate, see the inset of Fig. 1(b). The nature of the particle-film interaction is primarily governed by the size of the particle and the corresponding in-plane wave vector. To get an estimate of this number we assume that the particle diameter D is half a wavelength of the characteristic plasmon, thus $k_\parallel = 2\pi / \lambda_p = \pi / D$. For a particle of radius 30 nm this yields $k_\parallel = 5.2 \cdot 10^7$ m^{-1}. The circle marked S in Fig. 1(b) is placed at the energy and characteristic wave vector of this isolated-particle plasmon.

With a metal film present, the spectra in Fig. 1(a) typically display two maxima, a low-energy image-dipole peak and a high-energy particle mode. The position of the low-energy peak is very sensitive to the film thickness and, for most of the range of t_f values, shifts to higher photon energies with increasing film thickness (indicated by black crosses in Fig. 1 (b)), as does the bound plasmon mode of the film alone. For $t_f = 5$ nm we see a shoulder around 1.8 eV which then becomes more marked around 2 eV for $t_f = 10$ nm, and develops into a clear peak at 2.1 eV for $t_f = 18$ nm. Meanwhile, the peak position of the high-energy mode peak is only weakly dependent on the film thickness, and remains very close to the resonance position of an isolated particle. For the thickest film with $t_f = 50$ nm, the two peaks have essentially coalesced into a fairly broad feature. It is also instructive to see how the intensity of the low-energy peak develops as the film thickness increases. Since the existence of this peak relies on the formation of a mode involving coupled electron oscillations in both the particle and the film it is natural that the peak is weak for the thinnest films, since in this case there are relatively few electrons in the film that can be set in motion. As the film gets thicker, the presence of more electrons increases the intensity of the low-energy mode. However, for the $t_f = 50$ nm film we see a general decrease in the scattering intensity to the glass side since then the film starts to become opaque.

Figures 1(c) and 1(d) show vector plots of the real parts of the electric fields in the x- and z-directions, $Re\{E_x\}$ and $Re\{E_z\}$, in the xz plane for the case of $t_f = 10$ nm. At 2 eV (Fig. 1 (c)) the electric field is concentrated to the region around the gap between the particle and the film, and we see that an image dipole is excited in the metal film. At 2.4 eV (Fig. 1(d)), on the other hand, the particle has a dipole moment similar to what one would see on an isolated particle. But on top of that the interaction with the film induces additional charges so that also a quadrupole moment is formed on the particle. In both cases the charges at opposite sides of the particle-film gap are out of phase with each other, while the charges on opposite surfaces of the film are in phase with each other, i.e. it is basically only the bound film plasmons that are excited.

Insets in Figs. 1(c) and 1(d) show the far field radiation pattern into the glass side on the Fourier plane k_x-k_y, where $k_x = k_g \sin(\theta) \cos(\varphi)$, $k_y = k_g \sin(\theta) \sin(\varphi)$ and $k_g = 2\pi n / \lambda$ is wave number in glass, with λ the free-space wavelength. The inner, dashed green circle marks the border ($k_\parallel = k_{air}$) between propagating and evanescent waves in air, while the solid green circle marks the same border ($k_\parallel = k_g$) for waves in the glass. (We will sometimes refer to the region $k_\parallel < k_{air}$ as the allowed one, and the region $k_{air} < k_\parallel < k_g$ as the forbidden one.) At first sight the results here may seem surprising given that the incident light is polarized along the x direction and excites a dipole moment on the particle in that direction; yet, for a photon energy of 2 eV, most of the scattered radiation goes out in a direction along the x axis. However, we have to keep in mind that while our image of the Fourier plane just shows the x and y components of the wave vector, it indeed has a z component as well, and $k_x^2 + k_y^2 + k_z^2 = k_g^2$. Thus the strong maximum along the k_x axis near the dashed green circle corresponds to radiation into the glass substrate leaving the metal film at an angle somewhat larger than the glass critical angle 41.8 degrees. This radiation is generated by oscillating charges on the particle close to the metal film that excite an evanescent p-polarized wave on the air side of the film that is then converted to a propagating wave in the glass. This mechanism is quite naturally much more effective for the low-energy mode than the high-energy mode, since in the former case the oscillating charges on the particle are much closer to the metal film, which means that the coupling mediated by evanescent waves is stronger. The figure illustrates the consequences of this rather nicely. For 2 eV, the glass side radiation pattern shows a strong maximum along the x-axis between the two green circles. For 2.4 eV, in contrast, the maxima occur along the y-axis, as expected for dipole radiation. Turning our attention to the inner, allowed part of the Fourier image, $k_\parallel < k_{air}$, corresponding to propagating waves in air we see that the radiation patterns for the low-energy and high-energy modes are rather similar. Here most of the radiation goes out in directions perpendicular to that of the particle dipole moment.

A radiation pattern similar to the one seen for a photon energy of 2 eV in Fig. 1(c) was found also in the early experimental study of Hecht et al. using a SNOM tip as a localized light source near a gold surface [22]. The result is also consistent with the findings in terms of angular patterns of Kume et al. who used a setup that can be thought of as the reverse of the gedanken experiment we suggest here [23].
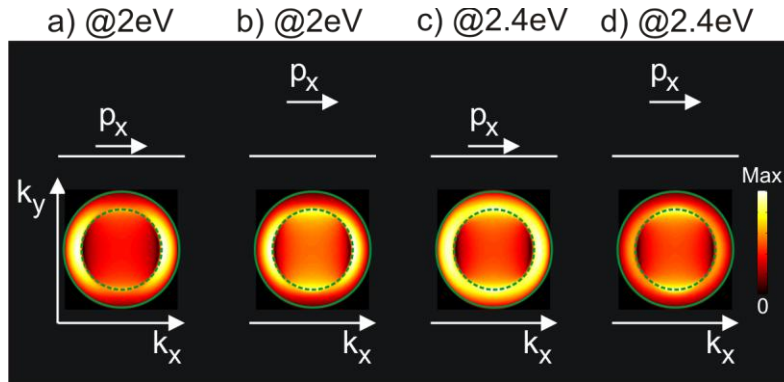

Fig. 2. Fourier images showing the radiation pattern into glass at 2 eV (a, b) and 2.4 eV (c, d) for x-oriented dipoles positioned in air above a 10 nm gold film at a glass substrate. The dipoles are positioned at 1 nm (a, c) and 31 nm (b, d) above the film, respectively.

We can get a basic understanding of the results in Fig. 1 from a model where a point dipole oriented along the x-axis is positioned above a 10 nm thick gold film on a glass substrate. The results of this model in terms of Fourier images are shown in Fig. 2, and the images in panels a) and d) agree qualitatively very well with those from Fig. 1. In general a dipole placed closer to the surface gives more radiation in the forbidden region along the x direction, since it interacts more effectively with the evanescent, p-polarized surface plasmon waves. A dipole placed further from the surface on the other hand gives more radiation along the y-axis because this requires coupling to s-polarized waves. This coupling is suppressed near the metal film, especially for the lower photon energy, as a result of destructive interference between the dipole and its image in the film.

In Fig. 3 we investigate how the scattering depends on the distance between the particle and the film. Figure 3(a) shows spectra for a gold sphere positioned at different distances d above an 18 nm thick gold film and Fig. 3(b) shows the far field radiation pattern into glass in the Fourier plane at 2.375 eV. With increasing distance d, the spectrum gradually transforms into the spectrum of a particle in air. If the particle is placed far away from the film, its dipole moment can oscillate on its own, without interacting strongly with the image dipole of the film. This yields a strong radiation intensity, in particular in allowed directions inside the inner circle of the Fourier image. At the same time, for large d, the interaction between the particle and the film is weak and the low-energy mode is absent from the spectrum in Fig. 3 (a). When the particle is moved closer to the metal film the interaction with the image dipole increases, and this leads to a reduction of the radiation intensity in allowed directions since the primary and image dipoles point in opposite directions and thus interfere destructively with each other. At the same time the radiation intensity in the forbidden area of the Fourier image increases with decreasing d. This can be understood from the discussion above; evanescent plasmon waves on the air side of the film play an essential role in mediating this radiation and of course this step is more effective for smaller particle-film distances. To summarize, changing the particle-film distance here leads to a shift in the directionality of the radiation pattern on the glass side from being mainly oriented perpendicular to the dipole direction for large separations to being oriented along the dipole direction for smaller d.
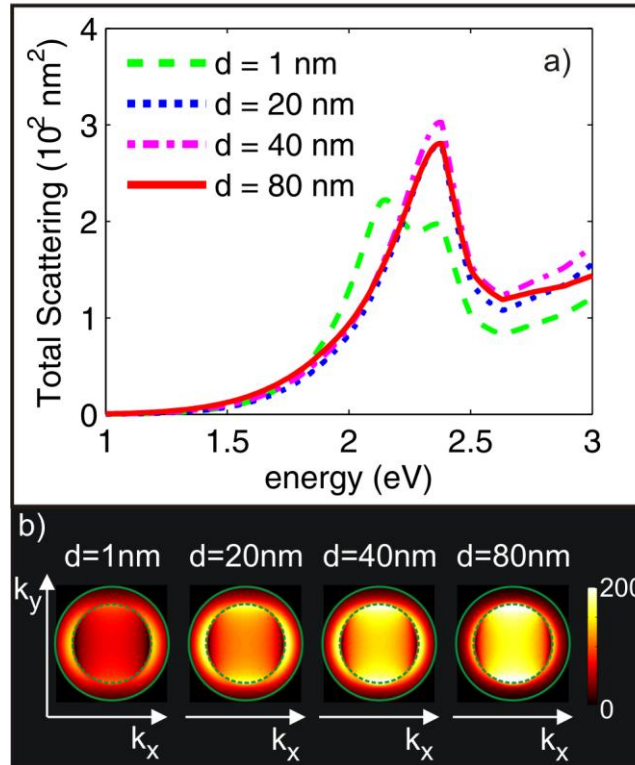
Fig. 3. (a) Scattering spectra for a gold sphere (R = 30 nm) in air above an 18 nm thick gold film on a glass substrate calculated for different particle-film distances *d*. (b) Fourier images showing the radiation pattern into glass at 2.375 eV for different *d*. We see a characteristic change of the pattern as *d* increases.

In Fig. 4 we turn to study scattering off a gold nanodisk separated from a gold film by a thin glass spacer layer. Figure 4(b) shows the dispersion relation for the layered vacuum/glass-spacer/gold-film/glass-substrate system shown in the inset. This plasmon dispersion relation is very similar to the one in Fig. 1(b), but a small energy downshift is noticeable due to the additional spacer layer. Figure 4(a) shows scattering spectra from a cylindrical gold nanodisk with diameter $D = 60$ nm and thickness $t = 20$ nm placed in air on top of the spacer layer. Here we see a considerable red-shift compared with the free-space case already when the nanodisk is placed on a glass substrate, compare the solid and dashed black curves. The reason is that the charges on the disk end up much closer to the substrate than the charges on the sphere did, and therefore we now have a stronger coupling with the image dipole. In the presence of the gold film we get two scattering resonance peaks, just as for the sphere. However, the energy split is much larger now for the reasons mentioned above; the low-energy mode yields a peak at about 1.2 eV for $t_f = 5$ nm. Increasing the film thickness causes both resonance peaks to blue-shift, i.e. these peaks shift in the same way as the bound plasmon mode of the film does when changing t_f. We also see that the intensity of the high-energy scattering peak falls off quite markedly as the film becomes thicker, while the scattering intensity from the low-energy mode increases to begin with but eventually falls off when the film starts becoming opaque (at $t_f = 50$ nm).
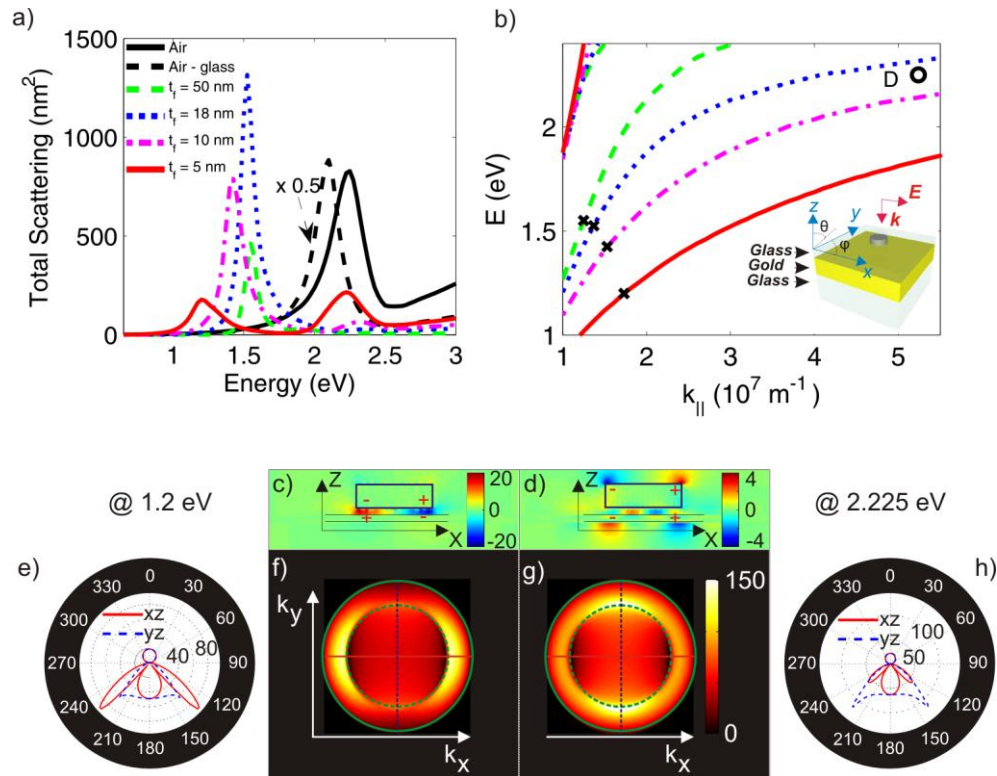
Fig. 4. (a) Scattering spectra for a gold nanodisk (D = 60 nm, t = 20 nm) placed on a 5 nm glass spacer layer on top of a gold film of thickness t_f. In addition, spectra for a nanodisk in air and at an air-glass interface are shown. (b) Dispersion relations similar to Fig. 1 (b), but with a spacer layer on top of the film (inset). (c, d) Real part of the z component of the electric field $Re\{E_z\}$ at energy 1.2 eV and 2.225 eV showing the charge distributions for the low-energy and high-energy modes for a 5 nm thick film, respectively. (e, h) Polar plots show the angular distribution of light scattered in the vertical xz and yz planes for (e) the low-energy and (h) the high-energy mode. (f, g) The corresponding Fourier images for (f) the low-energy and (g) the high-energy mode.

Figures 4(c) and 4(d) show the real part of the Z component of the electric field for the two scattering resonances at 1.2 eV and 2.225 eV, respectively, with a 5 nm thick gold film. The low-energy mode displays a dipole on the disk located towards the film side that induces an image dipole in the film. The main feature of the high-energy mode is a dipole located at the air side of the disk complemented by weaker charges induced at the bottom of the particle. These two figures also give a clue to why the intensities of the two scattering peaks develop the way they do as t_f increases. If the film is thin compared with the disk, the field from the disk will drive the film. Then the charges in the disk will mainly oscillate the same way as in a disk in free space, and consequently the "disk-like" high-energy mode will dominate the scattering. This is what we see in the t_f = 5 nm spectrum. However, as the film thickness increases, the roles are reversed; eventually the field from the charges in the film drives the particle instead and the strongly coupled low-energy mode grows in intensity, while the high-energy mode starts to disappear, in part because it is further blue-shifted into a spectral region with stronger damping due to interband transitions. In Fig. 4(a), for t_f = 50 nm essentially only the low-energy peak remains. Finally, Figs. 4(f) and 4(g) show the radiation patterns in the glass-side Fourier plane for the two scattering resonances. These agree very well with what we expect in view of the discussion of Fig. 1, the strongly coupled low-energy mode gives rise to strong scattering along the x axis into the forbidden part of the Fourier plane, while the disk-like high-energy mode yields a dipole-like pattern along the y axis and into the allowed part of the Fourier plane. In addition, Figs. 4(e) and 4(h) show polar plots for the scattering in

the vertical xz (parallel to the dipole orientation) and yz (perpendicular to the dipole orientation) planes, respectively. It is obvious that the difference between the two modes in terms of directionality is much more pronounced for the radiation that goes into the glass (downwards in these polar plots) than it is for the radiation into air.

4. Conclusions

We have presented a theoretical study of elastic light scattering from a gold nanoparticle placed closed to a thin gold film on a glass substrate illuminated under normal incidence. We are particularly interested in the directionality of the light scattered to the glass side of the film. We found that the coupled nanoparticle-metal film system possesses two localized modes built up through hybridization between the particle dipolar plasmon modes and the evanescent plasmon waves of the film. The high-energy mode mainly gives rise to an ordinary "particle-like" dipole radiation pattern whereas the low-energy "film-like" mode yields substantial scattering into directions closer to the particle dipole axis. The relative strength of the two scattering peaks can be modulated by changing the particle-film distance as well as the dielectric environment of the nanoparticle.

Acknowledgments